AMERICAN SOCIETY FOR MICROBIOLOGY | mSphere®

RESEARCH ARTICLE
Molecular Biology and Physiology

# Quantifying Oxygen Management and Temperature and Light Dependencies of Nitrogen Fixation by *Crocosphaera watsonii*

**Keisuke Inomura,[a] Curtis Deutsch,[a] Samuel T. Wilson,[b] Takako Masuda,[c] Evelyn Lawrenz,[c] Lenka Bučinská,[c] Roman Sobotka,[c] Julia M. Gauglitz,[d,e] Mak A. Saito,[e] Ondřej Prášil,[c] Michael J. Follows[f]**

[a]School of Oceanography, University of Washington, Seattle, Washington, USA
[b]Daniel K. Inouye Center for Microbial Oceanography: Research and Education (C-MORE), University of Hawaii, Honolulu, Hawaii, USA
[c]Institute of Microbiology, The Czech Academy of Sciences, Třeboň, Czech Republic
[d]Collaborative Mass Spectrometry Innovation Center, Skaggs School of Pharmacy and Pharmaceutical Sciences, University of California, San Diego, San Diego, California, USA
[e]Marine Chemistry and Geochemistry Department and Biology Department, Woods Hole Oceanographic Institution, Woods Hole, Massachusetts, USA
[f]Department of Earth, Atmospheric and Planetary Sciences, Massachusetts Institute of Technology, Cambridge, Massachusetts, USA

**ABSTRACT** *Crocosphaera* is a major dinitrogen ($N_2$)-fixing microorganism, providing bioavailable nitrogen (N) to marine ecosystems. The $N_2$-fixing enzyme nitrogenase is deactivated by oxygen ($O_2$), which is abundant in marine environments. Using a cellular scale model of *Crocosphaera* sp. and laboratory data, we quantify the role of three $O_2$ management strategies by *Crocosphaera* sp.: size adjustment, reduced $O_2$ diffusivity, and respiratory protection. Our model predicts that *Crocosphaera* cells increase their size under high $O_2$. Using transmission electron microscopy, we show that starch granules and thylakoid membranes are located near the cytoplasmic membranes, forming a barrier for $O_2$. The model indicates a critical role for respiration in protecting the rate of $N_2$ fixation. Moreover, the rise in respiration rates and the decline in ambient $O_2$ with temperature strengthen this mechanism in warmer water, providing a physiological rationale for the observed niche of *Crocosphaera* at temperatures exceeding 20°C. Our new measurements of the sensitivity to light intensity show that the rate of $N_2$ fixation reaches saturation at a lower light intensity ($\sim$100 $\mu$mol $m^{-2}$ $s^{-1}$) than photosynthesis and that both are similarly inhibited by light intensities of $>$500 $\mu$mol $m^{-2}$ $s^{-1}$. This suggests an explanation for the maximum population of *Crocosphaera* occurring slightly below the ocean surface.

**IMPORTANCE** *Crocosphaera* is one of the major $N_2$-fixing microorganisms in the open ocean. On a global scale, the process of $N_2$ fixation is important in balancing the N budget, but the factors governing the rate of $N_2$ fixation remain poorly resolved. Here, we combine a mechanistic model and both previous and present laboratory studies of *Crocosphaera* to quantify how chemical factors such as C, N, Fe, and $O_2$ and physical factors such as temperature and light affect $N_2$ fixation. Our study shows that *Crocosphaera* combines multiple mechanisms to reduce intracellular $O_2$ to protect the $O_2$-sensitive $N_2$-fixing enzyme. Our model, however, indicates that these protections are insufficient at low temperature due to reduced respiration and the rate of $N_2$ fixation becomes severely limited. This provides a physiological explanation for why the geographic distribution of *Crocosphaera* is confined to the warm low-latitude ocean.

**KEYWORDS** *Crocosphaera*, carbon, cell flux model, daily cycle, iron, light, nitrogen, nitrogen fixation, oxygen, photosynthesis, temperature

Nitrogen (N) availability is recognized as a growth-limiting factor for primary producers in the ocean (1–4), controlling the flow of carbon (C) through the ecosystem (5–7). Dinitrogen fixation ($N_2$ fixation) represents an important source of N that is

**Citation** Inomura K, Deutsch C, Wilson ST, Masuda T, Lawrenz E, Bučinská L, Sobotka R, Gauglitz JM, Saito MA, Prášil O, Follows MJ. 2019. Quantifying oxygen management and temperature and light dependencies of nitrogen fixation by *Crocosphaera watsonii*. mSphere 4:e00531-19. https://doi.org/10.1128/mSphere.00531-19.

**Editor** Grant R. Bowman, University of Wyoming



Address correspondence to Keisuke Inomura, ki24@uw.edu.

*[This article was published on 11 December 2019 with the sixth author's name presented incorrectly. The byline has been updated in the current version, posted on 30 January 2020.]*

**Received** 22 July 2019
**Accepted** 6 November 2019
**Published** 11 December 2019

estimated to account for nearly 50% of the fixed N input in the ocean (7). The microorganisms that fix $N_2$ are termed "diazotrophs" and are physiologically diverse, including unicellular, filamentous, and heterocystous cyanobacteria with life strategies that include symbiotic, free-living, and colonial forms (8). *Crocosphaera watsonii* is a major phototrophic diazotroph and makes a significant contribution to the pool of fixed N in oligotrophic environments of the subtropical and tropical Atlantic and Pacific oceans (9–12). Observations show that the niche of *Crocosphaera* is limited to the region above 20°C (12, 13). Similarly, laboratory culturing experiments show that *Crocosphaera* grow only above 20°C (14, 15).

The enzyme responsible for $N_2$ fixation, termed "nitrogenase," is highly sensitive to oxygen ($O_2$) (16, 17), thus necessitating careful $O_2$ management by diazotrophs (18). In particular, *Crocosphaera* is a cyanobacterium with oxygen-producing photosynthesis, and fixing both C and $N_2$ simultaneously would be a challenge. To circumvent the potential problem caused by $O_2$ production, *Crocosphaera* fix $N_2$ predominantly during the dark period in both laboratory (19–21) and natural (22) populations, thereby temporally segregating $N_2$ fixation from $O_2$-producing photosynthesis. However, $O_2$ in the ocean is mostly saturated (~200 $\mu$M in low latitudes) (23), and diurnal fluctuation of $O_2$ is relatively small (~10 $\mu$M) (24). Thus, even during the dark period, cells are likely to be exposed to a considerable influx of $O_2$. Even at 5% $O_2$ (~50 $\mu$M), nitrogenase activity decreases to less than 30% within 20 min (17). Thus, questions remain about how *Crocosphaera* protects nitrogenase against $O_2$.

$O_2$ management by *Crocosphaera* must be considered within the context of their distinct daily physiological cycle. One metabolic strategy to constrain $O_2$ is to sustain high rates of respiration in excess of the energetic demand during the night by using C stored from photosynthesis during the day (25). This distinct physiological cycle is paralleled by management of intracellular iron (Fe). *Crocosphaera* shuttles intracellular Fe between photosystems and nitrogenase during the daytime and the dark period to support photosynthesis and $N_2$ fixation, respectively. The nitrogenase complex in particular is completely degraded and resynthesized each day (21). Despite the significance of the intracellular Fe cycling, the quantitative models have not mechanistically included the cycling nor have they linked it with other metabolisms, i.e., those affecting C, N, and $O_2$. Developing a model which explicitly links Fe cycling to cellular metabolisms allows us to test how $O_2$ can be managed within the context of the distinct daily cycle of Fe, C, N, and $O_2$.

**Physiological model of *Crocosphaera*.** First, we describe a new model of the C, N, Fe, and $O_2$ budgets of *Crocosphaera,* and we then use it as a tool to explore the role of different $O_2$ protection mechanisms. A more detailed description of the model is found in Materials and Methods and in Text S1 in the supplemental material.

**Simulating the daily cycle of metabolism based on Fe translocation.** We quantify the daily metabolic cycle for *Crocosphaera* by developing a coarse-grained model of *Crocosphaera* (cell flux model of *Crocosphaera* [CFM-Croco]), as depicted in Fig. 1 (see Materials and Methods and Text S1 for details). A previous dynamic model of *Crocosphaera* was developed to examine the daily cycle of C and N in *Crocosphaera* driven by a cellular clock and time-dependent functions (26). In our model, we explicitly link Fe cycles to C, N, and $O_2$ metabolisms. As a starting point, we assume the total Fe constant within the cell and simulate the temporal variation of the fraction of Fe in different pools. During the light period, a predominant amount of Fe exists in photosystems contributing to photosynthesis. After sunset, Fe moves to nitrogenase, increasing the rate of $N_2$ fixation. Before sunrise, Fe moves back to photosystems, preparing for daytime photosynthesis. We linearly link the amount of Fe in photosystems with the rate of photosynthesis and that in nitrogenase with the rate of $N_2$ fixation leading to diurnal fluctuation of these metabolic rates. During the daytime, with photosynthesis, C storage (starch) is accumulated and fuels nitrogen fixation during the night. Nighttime metabolism also includes respiratory depletion of intracellular $O_2$, which depends on the amount of C storage and the temperature-dependent metabolic capacity.

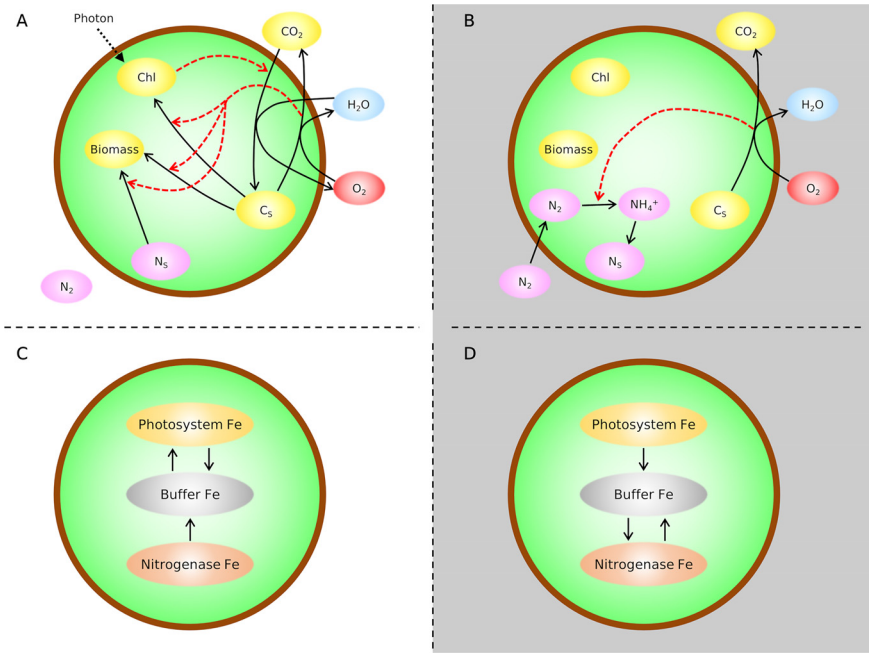


**FIG 1** Schematics of modeled C, N, $O_2$, and Fe fluxes. (A and B) C, N, and $O_2$ fluxes for light and dark periods, respectively. Black solid arrows represent material fluxes, red dashed arrows represent energy fluxes, and a black dotted arrow represents photon flux. C-based molecules are in yellow, N-based molecules are in pink, $O_2$ is in red, and $H_2O$ is in blue. $C_S$ and $N_S$, C and N storage, respectively; Chl, chlorophyll. (C and D) Fe fluxes (black solid arrows) for light and dark periods, respectively. The large circular frame indicates the cellular boundary.

**Quantifying the rate of $N_2$ fixation.** $N_2$ fixation is modeled as explicitly dependent on the intracellular concentration of nitrogenase, the size of the intracellular carbohydrate and fixed-N stores, the intracellular $O_2$ concentration, and the temperature. During the dark period at a fixed temperature, the rate of $N_2$ fixation ($N_{2fix}$; mol N cell$^{-1}$ h$^{-1}$) is assumed to be affected by the fluctuation of Fe, the respiratory depletion of intracellular $O_2$, and the storage of N and C as depicted in Fig. 2

$$N_{2fix} = A_{N2fix} Fe_N f_N\left(C_S, N_S, O_2^{cell}\right) \quad (1)$$

where $A_{N2fix}$ is a rate constant (mol N mol Fe$^{-1}$ h$^{-1}$), $Fe_N$ is the mass of Fe in nitrogenase (mol Fe cell$^{-1}$), and $f_N(C_S, N_S, O_2^{cell})$ scales the rate of N fixation between zero and its maximum value per nitrogenase ($A_{N2fix}$), based on the available C storage ($C_S$; mol C cell$^{-1}$) and N storage ($N_S$; mol N cell$^{-1}$) and the presence of intracellular $O_2$

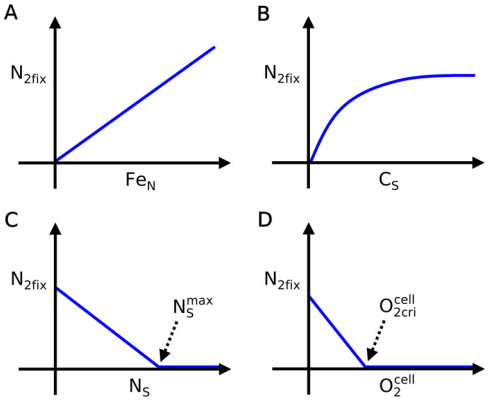


**FIG 2** Schematics of how each factor influences $N_{2fix}$ in the model. (A) $Fe_N$; (B) $C_S$; (C) $N_S$; (D) $O_2^{cell}$. $N_S^{max}$ is the maximum N storage capacity, and $O_{2cri}^{cell}$ is the critical $O_2$ concentration.

($O_2^{cell}$; mol $O_2$ $cell^{-1}$). Increasing nitrogenase concentrations (as proxied by $Fe_N$) increase the encounter rate of $N_2$ gas, with nitrogenase proportionally/linearly increasing $N_{2fix}$ (Fig. 2A). $C_S$ positively influences $N_{2fix}$, since it provides energy for $N_2$ fixation. We have assigned a saturating dependence (Michaelis-Menten type curve) to $C_S$ (Fig. 2B), the C substrate. On the other hand, we assume that $N_S$ negatively influences $N_2$ fixation (Fig. 2C), as reactive N is often observed to inhibit $N_2$ fixation (27–29). Intracellular $O_2$ ($O_2^{cell}$) also negatively influences $N_2$ fixation, since the proteins in the nitrogenase complex are sensitive to $O_2$ (16, 17) (Fig. 2D). We assign a critical $O_2$ concentration ($O_{2cri}^{cell}$) above which $N_2$ fixation does not occur, below which we assumed that $N_{2fix}$ increases linearly with decreasing $O_2^{cell}$. This assumption is to represent an *in vitro* experiment of nitrogenase activities, where there are rather gradual negative correlations between $O_2$ and activities of nitrogenase subunits (17).

**Simulating $O_2$ management.** To simulate the intracellular $O_2$ concentration, we assume a balance between diffusive flux into the cell and the respiratory $O_2$ consumption within it, which can be expressed as follows (18):

$$\left[O_2^{cell}\right] = \left[O_2\right] - \frac{r^2 \gamma_{net}}{3\kappa_{O_2}} \quad (2)$$

where $[O_2^{cell}]$ (mol $O_2$ $m^{-3}$) represents the intracellular concentration of $O_2$, $[O_2]$ (mol $O_2$ $m^{-3}$) is the environmental concentration of $O_2$, $r$ is the cell radius (m), $\gamma_{net}$ is the net respiration rate (respiration rate − photosynthesis) per cell volume (mol $O_2$ $m^{-3}$ $s^{-1}$), and $\kappa_{O2}$ is the effective $O_2$ diffusion coefficient ($m^2$ $s^{-1}$) which accounts for the diffusivity in both the molecular boundary layer surrounding the cell and a semipermeable cell membrane layers. In order to minimize $[O_2^{cell}]$, cells may live in low $[O_2]$ environments, increase cell size (increasing $r$), increase respiration (increasing $\gamma_{net}$), or decrease $O_2$ diffusivity through the cell membrane layers (decreasing $\kappa_{O2}$).

**Temperature dependence of metabolic processes.** To study why *Crocosphaera*'s niche exists mostly above 20°C, we use a commonly used temperature factor [$f_T(T)$] based on the Arrhenius equation (30, 31):

$$f_T(T) = \exp\left(A_T\left(\frac{1}{T_{ref}} - \frac{1}{T}\right)\right) \quad (3)$$

where $T$ is temperature (K), $T_{ref}$ is a reference temperature (K), and $A_T$ is a constant factor ($K^{-1}$). This factor independently modulates three key metabolic functions, namely, $N_2$ fixation, photosynthesis, and respiration, and simulates the daily integrated rates of metabolisms. We explore the significance of the temperature dependence of each metabolic component.

**Quantifying light dependence of metabolisms with laboratory measurements.** We model the dependence of photosynthesis on light using the commonly employed saturating functional form (32, 33) with photoinhibition:

$$f_I(I) = 1 - e^{A_I I} - \Omega(I) \quad (4)$$

where $I$ is light intensity ($\mu$mol $m^{-2}$ $s^{-1}$), $A_I$ is a light absorption/processing factor ($\mu mol^{-1}$ $m^2$ s), and $\Omega(I)$ is a photoinhibition term (dimensionless). We have also conducted laboratory measurements of $N_2$ fixation rates and photosynthetic electron transfer rates by *Crocosphaera watsonii* WH8501 for various light intensities (see Materials and Methods) and compared them with the model.

## RESULTS AND DISCUSSION

**Analysis of daily metabolic cycles.** We have simulated time-dependent laboratory cultures of *Crocosphaera* (25) and the linked Fe allocation within the cell (21). The model accurately predicted rates of photosynthesis and respiration both qualitatively and quantitatively for different $O_2$ concentrations in the culture (Fig. 3A): 20% (186 $\mu$M, the normal atmospheric composition and surface ocean concentration in tropics) and 5% (46 $\mu$M, one-quarter of the normal composition), as used in the previous laboratory experiment (25). The rate of photosynthesis was maximal during the middle of the day for both 20% and 5% $O_2$ values.

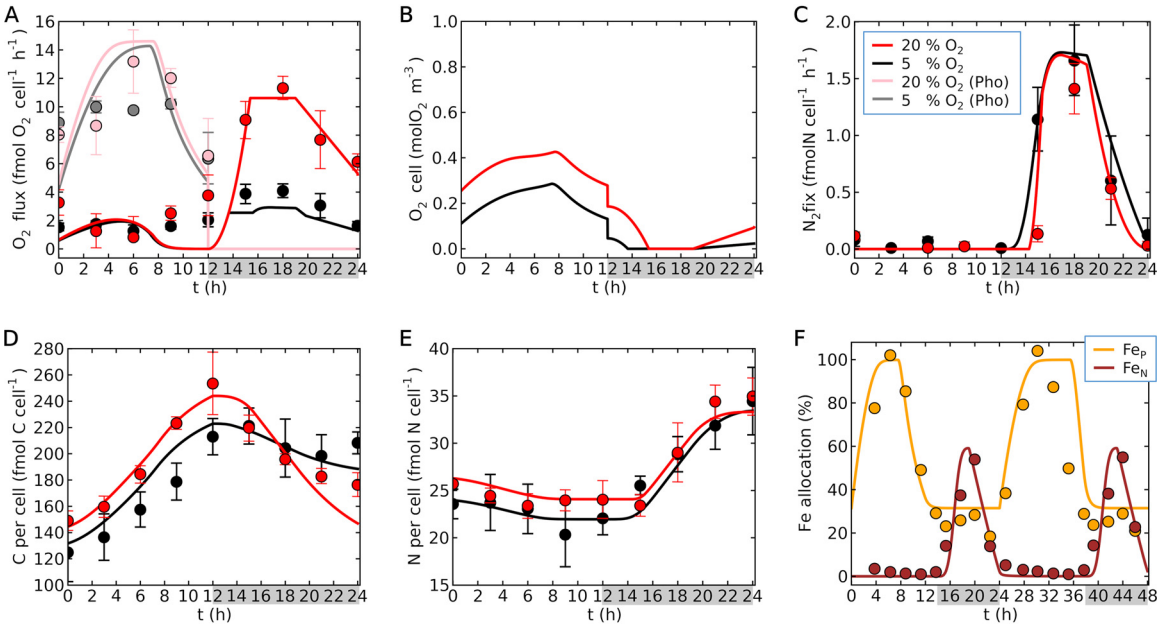


**FIG 3** Simulated diurnal cycle of *Crocosphaera* for different $O_2$ concentrations (curves) and laboratory data (circles). (A) $O_2$ fluxes based on photosynthesis (gray and pink) and respiration (red and black). Here, $O_2$ production is positive for photosynthesis, and $O_2$ consumption is positive for respiration. (B) $O_2$ concentrations in the cell. (C) $N_2$ fixation rates. (D) C per cell. (E) N per cell. (F) Fe allocation. In panels A to E, error bars are the standard deviations of laboratory data (25). Here, we used a theoretical factor of 3 for $C_2H_4$:$N_2$ (59). Red (or pink in panel A) is at 20% $O_2$, and black (or gray in panel A) is at 5% $O_2$. In panel F, Fe used by metabolism is based on quantitative protein data (21) for Fe in photosystems ($Fe_P$; orange) and nitrogenase ($Fe_N$; brown). In the model, the rest of the Fe exists in the buffer (an intracellular Fe storage). The key shown in panel C applies to panels A to E (pink and gray apply only to the photosynthesis (Pho) in panel A). In all panels, gray shading indicates dark periods. Temperature and light intensity are 28°C and 150 $\mu$mol m$^{-2}$ s$^{-1}$, respectively (21, 25).

The rate of photosynthesis was correlated with Fe cycles, since the rate is proportional to Fe in photosystems ($Fe_P$) (Fig. 3F); as the sun rises, Fe moves from the buffer (an intracellular Fe storage, e.g., ferritin and bacterioferritin [21]) to the photosystems, but in the afternoon, it starts moving back to the buffer, which was predicted by relating Fe to $C_S$. As $C_S$ increases and approaches maximum storage levels, there is no benefit to further photosynthesis. Therefore, the amount of photosystems was downgraded, and Fe was moved back to the buffer. We predicted a limited difference in photosynthesis between 5% and 20% $O_2$, consistent with laboratory data.

We also reproduced the observed daily cycle of respiration and showed that higher respiration rates occurred at 20% $O_2$ during the dark period due to respiratory protection (25). Because of this respiratory protection, intracellular $O_2$ concentrations decreased to almost zero during the middle of the night (Fig. 3B), leading to peak $N_2$ fixation during this period (Fig. 3C).

The data showed that $N_2$ fixation increased more quickly at 5% $O_2$ than at 20% $O_2$ during the early dark period and can be explained by the concentration of intracellular $O_2$. Based on the model, cellular $O_2$ was eliminated more quickly at 5% (Fig. 3B), reaching zero before 14 h, while such elimination occurs after 15 h for 20% $O_2$, thereby delaying $N_2$ fixation. This delay in $N_2$ fixation under normal $O_2$ conditions is widely observed both in the laboratory (19, 34) and in natural populations (22). This delay may reflect the extra time required for $O_2$ elimination, given that *Crocosphaera*'s *nifH* gene is transcribed following the initiation of the dark period (19, 21, 22), and both the model and laboratory data showed a much smaller delay in $N_2$ fixation in a low-$O_2$ environment. We capture this trend with the $O_2$ dependence of $N_2$ fixation (equation 1) (Fig. 2D); at 5% $O_2$, the intracellular $O_2$ is depleted quickly (Fig. 3B) and thus the rate of $N_2$ fixation increases earlier (Fig. 3C).

During the dark period, as the nitrogenase enzyme is synthesized, Fe moves from the buffer to nitrogenase, initiating $N_2$ fixation. As the dark period approaches dawn, Fe

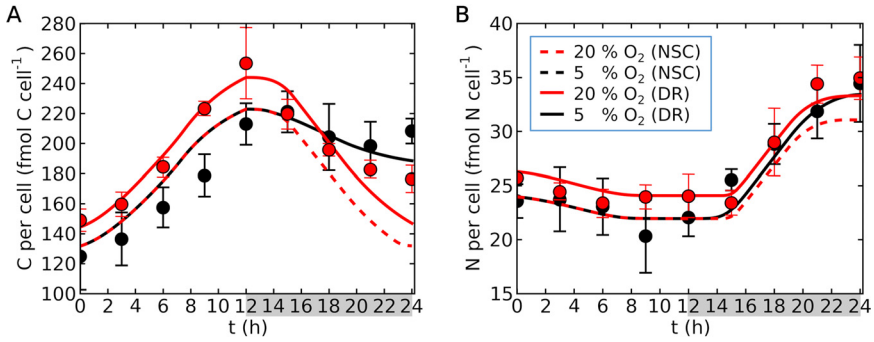


**FIG 4** Simulated daily cycle of *Crocosphaera* with no size change based on $O_2$ concentration. (A) C per cell. (B) N per cell. Curves represent simulations, and points with error bars (standard deviations) represent laboratory data (25). Here, we used a theoretical factor of 3 for $C_2H_4$:$N_2$ (59). Dashed curves represent the run with no size change (NSC), and solid curves represent the default run (DR) (as in Fig. 3). Red indicates 20% $O_2$, and black indicates 5% $O_2$. NSC and DR show the same results for 5% $O_2$ since the same size value is used. The key in panel B applies to both panels. Gray shading on the *x* axis indicates the dark period. Temperature and light intensity are 28°C and 150 $\mu$mol m$^{-2}$ s$^{-1}$, respectively (25).

begins moving back to the buffer, preparing for daytime photosynthesis through degradation of the nitrogenase protein complex (19, 21), accompanied by decreased respiration (Fig. 3A), leading to the drop in the rate of $N_2$ fixation (Fig. 3C) and increased intracellular $O_2$ (Fig. 3B). We can use the model to consider how *Crocosphaera*'s diel cycle might be regulated. If the C storage reservoir were to be the trigger for Fe transfer, we would expect C storage to be significantly reduced during the dark period. However, even at the end of the dark period, we predict a significant amount of C storage remaining in the cell. If N storage is the trigger, Fe should start moving earlier in the case of 5% $O_2$ than in the case of 20% $O_2$, as the cell fixes $N_2$ faster under low $O_2$. The data show, however, that the rate of $N_2$ fixation drops at almost the same time for the two $O_2$ cases. Also, the peak of $N_2$ fixation appears during similar time ranges among different studies (19, 21, 34). Finally, since *Crocosphaera* maintains the daily cycle even under continuous light (35, 36), it seems that the Fe transfer within *Crocosphaera* is largely controlled by a circadian clock that regulates key cellular functions. To further examine what controls Fe transfer, higher-resolution measurement of $N_2$ fixation (34) under various $O_2$ concentrations would also be useful.

Based on the metabolic rates (respiration, photosynthesis, cellular growth, and $N_2$ fixation), we computed the cellular C and N quotas (Fig. 3D and E). During the light period, the cells accumulate C, while during the dark period, C storage decreases due to respiration and $N_2$ fixation. During the light period, the data show that C accumulation is slightly greater for 20% $O_2$ than for 5% $O_2$; the model predicts this trend, with increased cell size for higher $O_2$ (thus, larger cell size for 20% $O_2$). During the dark period, however, it gets lower for 20% $O_2$ than for 5% $O_2$, due to higher respiration for $O_2$ management. Due to the larger cell size (discussed in "Sensitivity studies"), cells under 20% $O_2$ have higher N. However, at the end of the dark period, cellular N levels under these different $O_2$ concentrations get closer since the rate of $N_2$ fixation is higher for 5% $O_2$. The slight decrease in N during the early light period is due to cell division.

**Sensitivity studies.** In the following three sections, we describe sensitivity studies performed with the model to probe the significance of different $O_2$ protection strategies. To examine the effect of each strategy, we specifically turned off each $O_2$ management mechanism (size change, respiratory protection, and diffusion management) and the model results (cellular C, N, $O_2$ fluxes, and $N_2$ fixation rates) were compared with the default run with all the mechanisms present.

**Relationship between cell size and $O_2$.** An increase in cell size is a potential physiological strategy for *Crocosphaera*, since it decreases the surface-to-volume ratio, thereby decreasing passive $O_2$ uptake per volume (equation 2) (18). Adjusting the cell size based on $O_2$ concentrations facilitates replication of the laboratory data (Fig. 4).

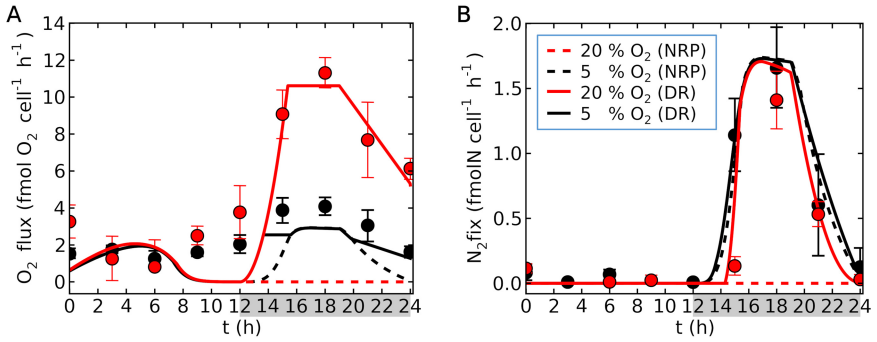


**FIG 5** Simulated daily cycle of *Crocosphaera* with no respiratory protection. (A) Respiration. (B) $N_2$ fixation. Curves represent simulations, and points with error bars (standard deviation) represent laboratory data (25). Here, we used a theoretical factor of 3 for $C_2H_4$:$N_2$ (59). Dashed curves represent the run with no respiratory protection (NRP), and solid curves represent the default run (DR) (as in Fig. 3). Red indicates 20% $O_2$, and black indicates 5% $O_2$. The key in panel B applies to both panels. Gray shading on the *x* axis indicates the dark period. Temperature and light intensity are 28°C and 150 $\mu$mol m$^{-2}$ s$^{-1}$, respectively (25).

During the light period, if the cell size is independent from $O_2$ concentration, the model shows identical values for C and N per cell for different $O_2$ concentrations, while the data show generally higher values for 20% $O_2$; as a result, more predictions are outside the error bars of the data, especially for C per cell (Fig. 4A). During the dark period, the data show a reverse effect in relation to C: the C per cell in 20% $O_2$ starts at a higher value but ends up at a lower value. This trend was reproduced only by including the size variation (Fig. 4A). N per cell is almost the same value at the end of the dark period, but the model with a fixed cell size shows much lower values in 20% $O_2$ outside the error bar (Fig. 4B). These results indicate that the cells acclimate to higher $O_2$ environments by adjusting their size. Recent studies have shown that there are two size classes of *Crocosphaera* (14, 22, 37). The model indicates that the larger cells have a significant advantage in $O_2$ management and might be a result of adapting to the high $O_2$ environments widespread in oceanic surface waters.

**Respiratory protection against $O_2$.** In order to examine whether respiratory protection is essential, we ran the model without respiratory protection (Fig. 5; see Fig. S1 in the supplemental material). In this case, respiration serves only to provide energy for $N_2$ fixation. At 5% $O_2$, the $N_2$ fixation rate is almost the same as that for the simulation with respiratory protection (Fig. 5B). Once the dark period initiates and photosynthesis stops, the cellular $O_2$ concentration drops low enough for $N_2$ fixation. As $N_2$ fixation initiates, respiration increases to provide energy, further decreasing intracellular $O_2$ to zero, until $N_2$ fixation peaks. On the other hand, at 20% $O_2$, even after the initiation of the dark period, the cellular $O_2$ concentration was still high (Fig. S1A), preventing $N_2$ fixation (Fig. 5B). The respiration rate was much lower than the laboratory values (Fig. 5A), especially at 20% $O_2$. Since there is no flux that consumes C at 20%, the model overestimated intracellular C (Fig. S1B). Together these results imply that respiratory protection is occurring in *Crocosphaera* and is essential for $N_2$ fixation at normal $O_2$ concentrations in the environment.

**Diffusion management.** A model-data comparison indicates that the diffusivity of the cell membrane layers must be extremely low relative to both the diffusivity in the molecular boundary layer and to the diffusivity of the cell membrane layers inferred from other $N_2$-fixing organisms. To achieve the results illustrated in Fig. 3, the effective diffusivity of $O_2$ across the cell membrane layers must be set to $1/(6.45 \times 10^4)$ of the diffusivity of $O_2$ in water. Previous studies of the heterotrophic and photoautotrophic diazotrophs *Azotobacter vinelandii* and *Trichodesmium* also inferred low cell wall permeability [$1/(1.27 \times 10^3)$ (18, 38) and $1/(1.60 \times 10^3)$ (39) of the diffusivity of $O_2$ in water, respectively], but the above predicted value for *Crocosphaera* is even lower. In contrast, the permeability of non-$N_2$-fixing bacterial cells is much higher [$1/(5.30 \times 10^2)$] (40).

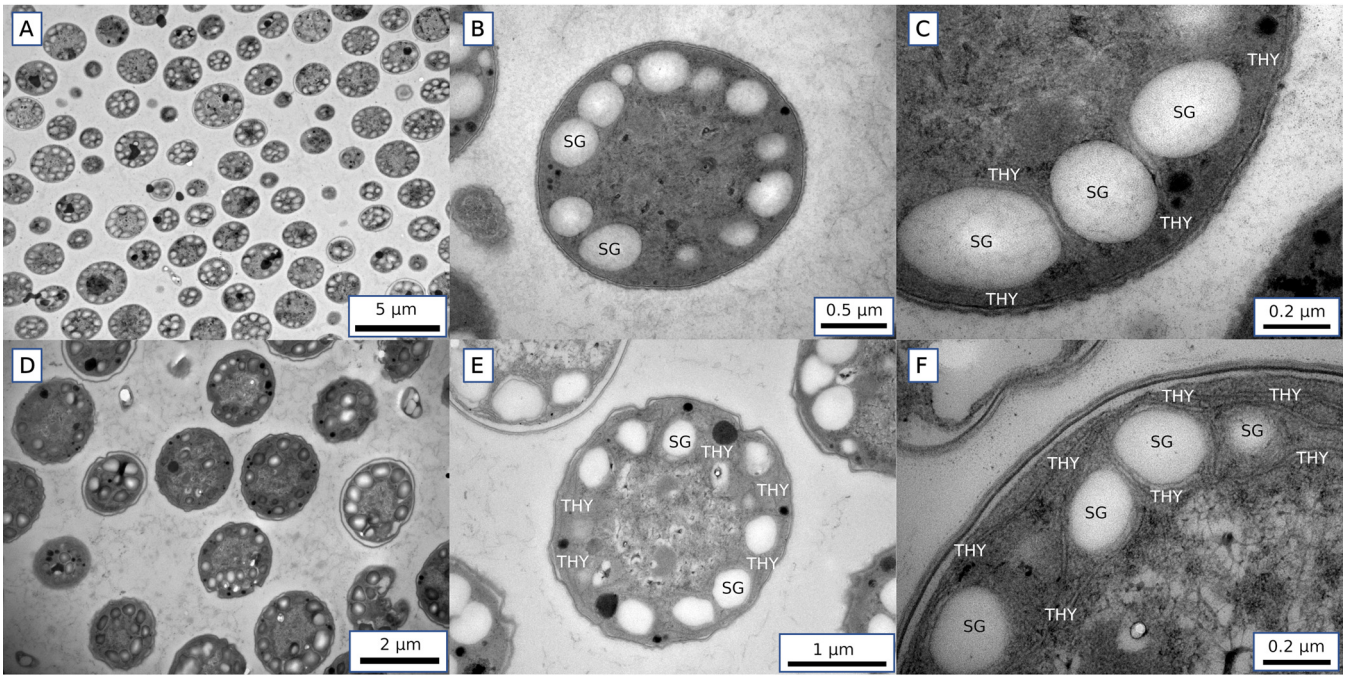


**FIG 6** Transmission electron micrographs of *Crocosphaera* cells harvested at the 6-h time point during the light period (A to C) and at the 6-h time point during the dark (D to F). Starch granules (SG) and thylakoid membranes (THY) are observed mostly on the edge of the cytosol. More-detailed images (C and F) show that SG are observed mostly between THY.

Applying the value inferred for *Azotobacter* results in poor simulations of the laboratory data (Fig. S2), significantly overestimating the respiration at 5% $O_2$ (Fig. S2A) and suppressing $N_2$ fixation (Fig. S2B) because the $O_2$ influx could not be matched. We conclude that *Crocosphaera* and other $N_2$-fixing microbes necessarily control the cell wall permeability for $O_2$; otherwise, $N_2$ fixation would be impossible. However, the required protection varies between species, and the details of this adjustment need to be further investigated.

One possibility is that carbohydrate storage may act as an $O_2$ barrier. As shown previously (41), during cell division, starch granules are accumulated near the cell membranes rather than spread evenly in the cytoplasm. Our original electron microscopy images of *Crocosphaera* ultrathin sections revealed that the location of the granules close to the membranes is well preserved in both the light and dark periods (Fig. 6). Since the starch granules are relatively rigid and have dense hydrophilic structures, it is likely that they act as a barrier against $O_2$ during the night. The images also show thylakoid membranes surrounding the granules (Fig. 6) (see also reference 41). Since respiration occurs on the thylakoid membranes as well as cellular membranes (42), such localization may make it possible for the cells to consume $O_2$ before it reaches the inner cytoplasm, as well as further physically decreasing the diffusivity of $O_2$.

Another possible barrier against $O_2$ diffusion is the production of extracellular polymeric substances (EPS), which may create a thick hydrophilic layer, where the diffusion of $O_2$ molecules is reduced. It has been hypothesized that *Azotobacter vinelandii* excrete alginate (one kind of EPS) to decrease the passive $O_2$ uptake and thus protect nitrogenase (43). Its effect on $N_2$ fixation has been further studied using quantitative modeling (18) and laboratory studies (44), supporting the hypothesis. In a batch culture, *Crocosphaera* produce EPS roughly proportional to their growth (37) and the production of EPS increases during the dark period (41). Given these findings, we hypothesize that the EPS produced by *Crocosphaera* plays an important role in reducing $O_2$ diffusion. Recent observations suggest that hopanoid lipids may also play a role in diffusion management, as they have biochemical properties that potentially decrease

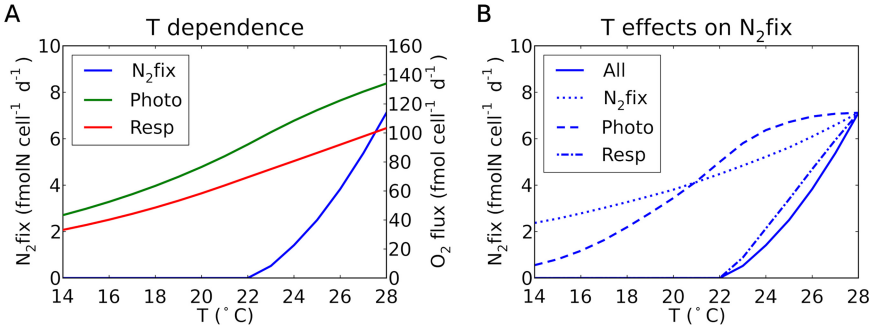


**FIG 7** Simulated temperature dependence on $N_2$ fixation, photosynthesis, and respiration. (A) Simulated temperature dependence on these metabolic fluxes when the temperature function is assigned to all of these fluxes. $N_2$fix, $N_2$ fixation; Resp, respiration; Photo, photosynthesis. (B) Impact of each temperature dependence on $N_2$ fixation rate. The solid curve represents when all three fluxes are temperature dependent. The other curves represent when only one of these fluxes is temperature dependent (see the key in the figure; i.e., $N_2$fix, Photo, and Resp indicate that the temperature function is assigned only to $N_2$ fixation, photosynthesis, and respiration, respectively). A light intensity of 150 $\mu$mol $m^{-2}$ $s^{-1}$ is used (25). Also, a saturating $O_2$ concentration is used based on the specified temperature and a salinity of 35 (60). The temperature dependence of diffusivity is given based on Walden's rule (61) and the temperature-dependent viscosity of water (62). The diffusivity of the cell membrane layers is assumed to be proportional to that of water (18).

the permeability to extracellular $O_2$ and hopanoid synthesis genes are specifically observed in non-heterocyst-forming cyanobacterial diazotrophs (45).

**Temperature dependence of $N_2$ fixation.** As we illustrate below, the model suggests that the temperature dependence of $N_2$ fixation, and thus the fitness of *Crocosphaera*, is largely explained by the temperature dependence of respiration. $N_2$ fixation by *Crocosphaera* is observed to have a strong dependence on temperature. Cell-specific rates of $N_2$ fixation are maximal at approximately 30°C and decrease to almost zero at 22°C (15). These laboratory-derived physiological observations are supported by field observations of *Crocosphaera* being most prevalent in warm oceanic regions above 20°C (12, 13).

In the model, $N_2$ fixation, photosynthesis, and respiration are each modeled with independent, Arrhenius equation-like temperature dependence (equation 3). By employing these in combination, the model replicates the observed temperature dependence of $N_2$ fixation (Fig. 7A). We tested which temperature dependence has the strongest effect by applying equation 3 to only one of the metabolisms (Fig. 7B). The results show that the temperature dependence on respiration has the strongest effect, closely representing the predicted results with all the temperature dependences. This indicates that the negative effect of temperature on $N_2$ fixation is largely due to decreased rates of respiration being insufficient to draw down intracellular $O_2$, and therefore nitrogenase is unable to fix $N_2$. A decrease in the rate of respiration will also decrease the supply of energy for nitrogenase. Decreased temperature will also have effects on other related metabolic processes, such as a direct effect on the rate of enzymatic activity of nitrogenase and a decrease in photosynthesis and therefore less C storage for respiration (Fig. 7B). All of these impacts, however, turned out to be smaller than the decrease in respiratory protection against $O_2$.

**The rate of $N_2$ fixation maximized at moderate light intensity.** To examine light dependence on $N_2$ fixation for *Crocosphaera*, we have simulated the rate of $N_2$ fixation at various light intensities. In the model, the light intensity influences the rate of photosynthesis based on the equation of light saturation and photoinhibition (equation 4). The model shows that the rate of $N_2$ fixation increases at low light intensity due to increased photosynthesis and, thus, increased C storage (Fig. 8A). However, despite photosynthesis rates increasing with light intensities up to ~700 $\mu$mol $m^{-2}$ $s^{-1}$ (Fig. 8B), $N_2$ fixation saturates at a relatively low light intensity (~100 $\mu$mol $m^{-2}$ $s^{-1}$) (Fig. 8A), since it becomes limited by the availability of nitrogenase (here proxied by $Fe_N$). This prediction is confirmed by our original measurements of the rates of

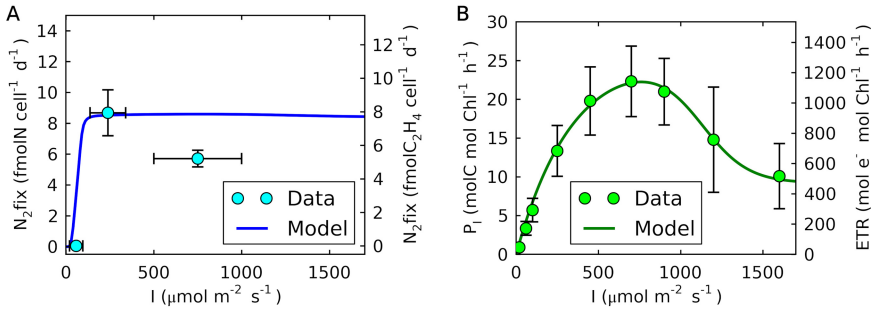


**FIG 8** Experimental data and model simulation of the light dependence of daily integrated rates of $N_2$ fixation and photosynthesis of *Crocosphaera*. (A) Simulated light dependence of the $N_2$ fixation rate of *Crocosphaera* at 20% $O_2$ (left axis) compared with the acetylene reduction data obtained in this study (right axis). (B) Simulated light dependence of the photosynthesis rate (left axis) compared with the average daytime ETR (electron transfer rate) measured in this study (right axis). Error bars represent the standard deviations of the samples. A temperature of 28°C was used.

acetylene reduction (proxy for $N_2$ fixation) and ETR (photosynthetic electron transfer rate) for various light intensities from this study. Above 140 $\mu$mol $m^{-2}$ $s^{-1}$, the rate of $N_2$ fixation becomes stable despite the significant increase in ETR.

Our measurements also show that above certain light intensities, both of the rates ($N_2$ fixation and photosynthesis) start dropping (Fig. 8), likely due to photoinhibition. These results may explain why the maximum population of *Crocosphaera* is often observed below the surface but above a depth of 50 m (12, 13), where they can receive moderate light intensities (100 to 400 $\mu$mol $m^{-2}$ $s^{-1}$), enough for $N_2$ fixation without photoinhibition. The model resolves photoinhibition, capturing the trend in ETR (Fig. 8B). However, it does not predict the observed decrease in $N_2$ fixation under strong light, despite the drop in photosynthesis above 700 $\mu$mol $m^{-2}$ $s^{-1}$, meaning that the rate of photosynthesis or the level of C storage cannot explain the decreasing trend in $N_2$ fixation (Fig. 8A). This indicates that high light intensity rather directly inhibits nitrogen fixation, potentially by damaging machinery for nitrogenase synthesis or subunits of nitrogenase before its assembly.

**Conclusions.** We have developed a coarse-grained model of *Crocosphaera* (CFM-Croco) and simulated a daily cycle of *Crocosphaera* metabolism with distinct C, N, $O_2$, and Fe fluxes. The model mechanistically links the diurnal cycle of Fe with that of C, N, and $O_2$, reproducing published observations (21, 25). This indicates that including the Fe cycle is essential for simulating the diurnal cycle of *Crocosphaera* metabolism and nutrient fluxes. The model results suggest that *Crocosphaera* employs multiple mechanisms to manage intracellular $O_2$: size change, respiratory protection, and decreased diffusivity. Since respiratory $O_2$ management is crucial for $N_2$ fixation, the temperature dependence of respiration has a significant impact on $N_2$ fixation, which provides a hypothesis for the strong temperature constraint on their growth and niche in the environment. The light dependence of photosynthesis does not give an advantage to $N_2$ fixation under extremely high light due to photoinhibition and limitations on nitrogenase concentration, the latter of which may be constrained by the intracellular space. This indicates that the optimum depth is likely not at the very surface, despite the potentially highest availability of Fe dust.

## MATERIALS AND METHODS

**Cell flux model of *Crocosphaera*.** Here, we describe the algorithms employed to implement the model. The model schematic is depicted in Fig. 1. Time-dependent equations are given to describe the rates of change in each of the macromolecular pools (Table 1). The fluxes between macromolecular pools are quantified at each time step. The time-dependent equations (Tables 1 and 2) are advanced in finite time steps, updating the status of the cells. Parameter values and nomenclature with units are available in Tables S1 and S2 in the supplemental material, respectively.

**C, N, and $O_2$ metabolism.** In order to compute the time variation of intracellular C, N, and $O_2$ pools and the cell density, we consider the chemical fluxes that impact them. Specifically, we include time variation of $C_S$, cell population density ($X$) based on biomass production, $N_S$, and $O_2$ (equations given in

**TABLE 1** Fundamental relations of C-, N-, and $O_2$-based molecules

| Equation[a] | Equation no. |
|---|---|
| $\frac{dC_S}{dt} = P_I\mathrm{Chl} - \lambda(1+E) - P_{CO2}^{N2fix} - P_{CO2}^{RP} - Exc$ | 5 |
| $\frac{dX}{dt} = \frac{X\lambda}{Q_C}$ | 6 |
| $\frac{dN_S}{dt} = N_{2fix} - \lambda Y_{bio\text{-}all}^{N:C}$ | 7 |
| $\frac{dO_2}{dt} = P_{O2} - R_{O2} + V_{O2}$ | 8 |

[a]$C_S$, C storage; *t*, time; $P_I$, photosynthesis rate per chlorophyll; Chl, chlorophyll; λ, biomass production rate; *E*, conversion factor of biomass production to biosynthetic $CO_2$ production; $N_{2fix}$, $N_2$ fixation rate; $P_{CO2}^{N2fix}$, $CO_2$ production due to electron donation to and respiratory energy production for $N_2$ fixation; $P_{CO2}^{RP}$, $CO_2$ production due to respiratory protection; *Exc*, C excretion rate; *X*, population density of cells; $Q_C$, cellular C quota; $N_S$, N storage per cell; $Y_{bio\text{-}all}^{N:C}$, N:C of biomass including storage; $O_2$, $O_2$ per cell; $P_{O2}$, $O_2$ production rate; $R_{O2}$, respiration rate; $V_{O2}$; $O_2$ exchange by diffusion.

Table 1 and schematics given in Fig. 1A and B). The balance in C storage pool $C_S$ (equation 5) is based on the balance among photosynthesis ($P_I$ Chl), biomass production (λ), biosynthetic $CO_2$ production (*E*λ), $CO_2$ production for $N_2$ fixation ($P_{CO2}^{N2fix}$), $CO_2$ production due to respiratory protection ($P_{CO2}^{RP}$), and C excretion (*Exc*). Cellular C and N are the sum of the baseline biomass and the C and N storages, respectively.

We assume that biomass production is used for the production of new cells, which drives the time change in population density (equation 6). Biomass production is supported not only by C but also by N. Thus, we consider the effect of biomass production on $N_S$ ($\lambda Y_{bio\text{-}all}^{N:C}$) (equation 7), which is balanced by $N_2$ fixation ($N_{2fix}$). Finally, the $O_2$ budget is based on photosynthesis ($O_2$ production rate [$P_{O2}$]), the respiration rate ($R_{O2}$), and the diffusive exchange of $O_2$ ($V_{O2}$) (equation 8).

Since the metabolism differs between the light and dark periods, we employed different parameterizations of the fluxes in Table 1 at different times of day. Specifically, $P_I$, λ, *Exc*, and $P_{O2}$ are unique to the light period, and $N_{2fix}$, $P_{CO2}^{N2fix}$, and $P_{CO2}^{RP}$ are specific to the dark period.

In order to solve the model equations, we have applied a finite-difference method to equations 5 to 7. Since the time scale of $O_2$ concentration is small relative to that of other metabolites (C, N, Fe), we have assumed a pseudo-steady state; thus, $O_2$ uptake and $O_2$ production are always balanced by respiration. For the calculation of fluxes that influence the time variation of each pool, we consider the size of the elemental pools and $O_2$ concentrations (the details of the flux calculations are described in Text S1 in the supplemental material).

**Fe metabolism.** The rates of C and $N_2$ fixation both depend on the Fe allocation to the enzymes which mediate those processes. Here, we model the time-dependent allocation to those Fe pools. The time-dependent equations for the Fe system are given in Table 2. We assume that the exchange of Fe

**TABLE 2** Fundamental relationships of Fe-related molecules

| Equation[a] | Equation no. |
|---|---|
| $\frac{dFe_P}{dt} = F_B^P - F_P^B$ | 9 |
| $\frac{dFe_B}{dt} = -F_B^P + F_P^B - F_B^N + F_N^B$ | 10 |
| $\frac{dFe_N}{dt} = F_B^N - F_N^B$ | 11 |
| $\frac{d\mathrm{Chl}}{dt} = (F_B^P - F_P^B)Y_{photo}^{Chl:Fe}$ | 12 |

[a]$Fe_P$, Fe in the photosystems; $F_B^P$ and $F_P^B$, translocation of Fe from the buffer to the photosystem and vice versa; $Fe_B$, Fe in the buffer; $F_B^N$ and $F_N^B$, translocation of Fe from the buffer to nitrogenase and vice versa; $Fe_N$, Fe in nitrogenase; $Y_{photo}^{Chl:Fe}$, Chl:Fe in the photosystems.

between photosystems and nitrogenase is mediated by an Fe buffer, such as bacterioferritin protein (Fig. 1C and D) (21). Thus, the time variation of Fe in the photosystems is based on its exchange with the buffer Fe pool (equation 9). The buffer Fe pool is influenced not only by the Fe from the photosystems but also by the exchange of Fe with nitrogenase (equation 10). The Fe allocation to nitrogenase results from the balance between the loss to and gain from the buffer (equation 11).

**Connecting Fe fluxes to C, N, and $O_2$ fluxes.** The amount of Fe in photosystems ($Fe_P$) proportionally influences photosynthesis, thus impacting C and $O_2$ fluxes. We have assumed that the ratio of chlorophyll to Fe in a photosynthetic apparatus (mol C mol $Fe^{-1}$) is constant ($Y_{photo}^{Chl:Fe}$); thus, the balance in chlorophyll is proportional to the balance in photosystem Fe (equation 12). The amount of chlorophyll in turn influences the rate of photosynthesis (equation 5). The rate of $N_2$ fixation ($N_{2fix}$) is assumed to be proportional to the amount of nitrogenase proxied by Fe in nitrogenase ($Fe_N$). Thus, through the rate of $N_2$ fixation, $Fe_N$ influences C and N fluxes, and through the associated respiration providing energy for $N_2$ fixation, it can influence $O_2$ fluxes.

In order to calculate the amount of Fe pools and chlorophyll, we applied a finite-difference method to equations 9 to 12. For the computation of Fe fluxes, we considered various factors, such as the size of the Fe pool of the origin and the destination, time, $O_2$ concentration, and carbohydrate storage. Fe fluxes are parameterized based on these factors to reproduce the laboratory observations (21) (Fig. 3F) (see Text S1 in the supplemental material).

**Differentiating light and dark periods.** To reflect a distinct diurnal cycle of *Crocosphaera*, we resolve differences in metabolic configuration during the day and night; some fluxes in Tables 1 and 2 are specific to a certain time of day. The schematics of which flux applies to each time period are illustrated in Fig. 1. The following section broadly describes the day-night differentiation. The detailed fluxes are described in Text S1.

**Light period.** During the light period, cells can harvest light and fix C, accumulating C storage and producing biomass (Fig. 1A). However, $N_2$ fixation is small and accordingly respiratory protection is also small. For the N source for biomass production, the cell relies on N storage. To reflect this, all the terms in equations 5 to 8 (Table 1) are used except $N_{2fix}$, $P_{CO2}^{N2fix}$, and $P_{CO2}^{RP}$ (~0). Also, we assume that the translocation of Fe from the buffer to nitrogenase ($F_B^N$) is ~0, since no $Fe_N$ was observed during the light period (21); this assumption depletes $Fe_N$ (Fig. 1C).

**Dark period.** During the dark period, photosynthesis does not occur, but the cell uses stored C for respiration and $N_2$ fixation (Fig. 1B). Also, we assume that biomass production and excretion do not occur. Thus, in equation 5, $P_l = \lambda = Exc = 0$. This assumption allows accumulating N storage with $N_2$ fixation, as observed previously (25). According to the observed targeted proteomics (21), there is limited net Fe flux to the photosystems, and we assume that the translocation of Fe from the buffer to the photosystem ($F_B^P$) is zero. This assumption creates the flow of Fe from photosystems to nitrogenase (Fig. 1D), increasing the rate of $N_2$ fixation during the early dark period. During the later dark period, we assume that $F_B^N$ is ~0, and the model forces the movement of Fe from nitrogenase to buffer as predicted (21).

**Simulating temperature and light dependences on metabolisms.** The temperature dependence is simulated based on applying a temperature factor $f_T(T)$ (equation 3) to $N_2$ fixation, photosynthesis, and respiration. To test the effect of temperature dependence on each metabolism, we applied $f_T(T)$ to only one of these metabolisms and plotted the rate of $N_2$ fixation (Fig. 7B). To represent the light dependence of photosynthesis, we have applied a light factor, $f_l(I)$, (equation 4) to the maximum rate of photosynthesis.

**Preparing *Crocosphaera watsonii* WH8501.** Stock cultures of *Crocosphaera watsonii* WH8501 were obtained from the Culture Collection Yerseke (The Royal Netherlands Institute for Sea Research, Yerseke, The Netherlands; strain number CCY 0601). The cells were maintained in N-free YBC-II medium (46) at 28°C in glass flasks under constant white light of 150 $\mu$mol $\mu m^{-2}$ $s^{-1}$ using a 12-h:12-h light-dark (12L:12D) cycle. At the beginning of each experiment, the cultures were transferred into flat-panel photobioreactors (FMT150; Photon System Instruments, Brno, Czech Republic) (47) with a sinusoidal 12L:12D growth irradiance peaking at 400 $\mu$mol $m^{-2}$ $s^{-1}$ with aeration. Cultures were acclimated to these conditions and maintained in exponential growth for at least 5 generations (about 15 days).

**Transmission electron microscopy.** *Crocosphaera* cells (~$10^8$ cells $ml^{-1}$) were harvested by centrifugation (5 min at 5,000 × *g*). The cells were resuspended in 1 volume of the growth medium mixed 1:1 with 5% (vol/vol) glutaraldehyde fixative in 0.2 M cacodylate buffer, pH 7.2. After 15 min of rotary shaking at room temperature, cells were transferred to 0.1 M cacodylate buffer containing 2.5% (vol/vol) glutaraldehyde and fixed overnight at 4°C. Pelleted cells were washed with cacodylate buffer and postfixed with 1% (wt/vol) osmium tetroxide for 2 h. After washing steps with the same buffer, cells were dehydrated through a graded series of acetone, embedded in low-viscosity Spurr resin (EMS), and polymerized at 60°C for 48 h. Ultrathin sections of 60 nm were cut using an ultramicrotome (UCT, Leica). Sections were collected on Formvar-coated copper grids and stained with 1% (wt/vol) aqueous uranyl acetate for 10 min and with Sato's lead citrate for 3 min (48). Prepared sections were examined in a JEOL 1010 transmission electron microscope (JEOL) equipped with a Mega View III camera (SIS). Acquired pictures were analyzed by ImageJ software (49).

**$N_2$ fixation measurements.** To determine the rates of $N_2$ fixation by acetylene reduction assays (50), 5 ml of cell suspensions grown under different light intensities were dispensed into HCl-rinsed glass vials. After each vial was sealed with a septum, 10 ml of acetylene gas (99.7% [vol/vol]; Linde Gas) was injected by replacing the same volume of headspace. The samples were incubated at 28°C in the dark for 12 h. Subsamples of the headspace were taken immediately after acetylene addition and then at the end of the incubation to measure their ethylene content with a flame ionization gas chromatograph (HRGC

5300; Carlo Erba Instruments). Ethylene production during the incubation was analyzed, and produced ethylene was calculated according to Breitbarth et al. (51).

**Variable-fluorescence light response curves.** The diel changes in the dependence of photosynthesis on light intensity was assessed with photosynthesis versus irradiance (P versus E) curves using the electron transfer rate (ETR) through photosystem II as a photosynthesis proxy. Cells were harvested in 2-h intervals throughout the diel cycle (52). Samples were acclimated to the dark for 10 min and placed inside a FL3500 fast repetition rate (FRR) fluorometer (Photon Systems Instruments, Czech Republic) maintained at the same temperature as the stock cultures. A series of 100 simultaneous blue (463 nm) and amber (617 nm) flashes of 1-$\mu$s duration was applied to induce a single turnover of the reaction centers of photosystem 2 (RCII) at 10 different light intensities ranging from 0 to 1,600 $\mu$mol quanta $m^{-2}$ $s^{-1}$ (0 to 840 $\mu$mol quanta $m^{-2}$ $s^{-1}$ of blue light combined with 0 to 600 $\mu$mol quanta $m^{-2}$ $s^{-1}$ of amber light). The resulting fluorescence light curves were fitted to the model of Kolber et al. (53) to derive the maximum ($F_m'$), operational ($F'$), and minimum ($F_o'$) fluorescence values at given actinic light, the effective PSII absorption cross-section ($\sigma_{PSII}$), and the connectivity between photosystems ($p$). These parameters were then used to calculate the ETR (54):

$$\mathrm{ETR} = \sigma_{\mathrm{PSII}} \times n_{\mathrm{PSII}} \times \frac{F_q'}{F_v'} \times \Phi_{\mathrm{RCII}} \times E \tag{13}$$

where $E$ is the intensity of the actinic light, $\Phi_{RCII}$ is the quantum yield of photochemistry within RCII [taking constant values of 1 mol $e^-$ (mol photons$^{-1}$)], $F_q'$ is variable fluorescence in the light ($F_m' - F'$), $F_v'$ is the maximal variable fluorescence in the light ($F_v' = F_m' - F_o'$), and $n_{PSII}$ is the ratio of functional reaction centers of PSII to total chlorophyll *a* (55, 56).

The ETR values were then plotted versus irradiance and modeled after the reports of Eilers and Peeters (57) and Silsbe and Kromkamp (58) to derive the maximum ETR ($ETR_{max}$), the initial slope of the P versus E curve, and the light saturation point of the ETR ($E_k$).

**Data availability.** The model developed in this paper as well as the plotted data have been uploaded in Zenodo/GitHub and is freely available from https://zenodo.org/record/3265448.

## SUPPLEMENTAL MATERIAL

Supplemental material for this article may be found at https://doi.org/10.1128/mSphere.00531-19.

**TEXT S1**, PDF file, 0.3 MB.

**FIG S1**, TIF file, 0.4 MB.

**FIG S2**, TIF file, 0.7 MB.

**TABLE S1**, PDF file, 0.2 MB.

**TABLE S2**, PDF file, 0.2 MB.

## ACKNOWLEDGMENTS

We thank Stephanie Dutkiewicz and Sallie W. Chisholm for useful discussion, Martin Lukeš for technical assistance for the $N_2$ fixation measurement, and the members of Writing and Communication Center at MIT for their advice on writing.

This research was supported by the Japan Student Service Organization (JASSO) (grant L11171020001 to K.I.), the Gordon and Betty Moore Foundation (grant GBMF 3775 to C.D. and grant GBMF 3778 to M.J.F.), the U.S. National Science Foundation (grant OCE-1756524 to S.T.W., grant OCE-1558702 to M.J.F., and grant OCE-PRF 1421196 to J.M.G), the Simons Foundation (Simons Postdoctoral Fellowship in Marine Microbial Ecology award 544338 to K.I., Simons Collaboration on Ocean Processes and Ecology award 329108 to M.J.F., Simons Collaboration on Computational BIOgeochemical Modeling of Marine EcosystemS [CBIOMES] award 549931 to M.J.F.), the Czech Science Foundation (GAČR) (grant 16-15467S to O.P.), and the National Sustainability Programme (NPU) (grant LO1416 Algatech plus to O.P.).

The funders had no role in study design, data collection and interpretation, or the decision to submit the work for publication.

## REFERENCES

1. Thomas WH. 1970. On nitrogen deficiency in tropical pacific oceanic phytoplankton: photosynthetic parameters in poor and rich water. Limnol Oceanogr 15:380–385. https://doi.org/10.4319/lo.1970.15.3.0380.
2. Thomas WH, Owen RW. 1971. Estimating phytoplankton production from ammonium and chlorophyll concentrations in nutrient-poor water of the eastern tropical Pacific Ocean. Fish Bull 69:87–92.
3. Ryther JH, Dunstan WM. 1971. Nitrogen, phosphorus, and eutrophication in the coastal marine environment. Science 171:1008–1013. https://doi.org/10.1126/science.171.3975.1008.
4. Caperon J, Meyer J. 1972. Nitrogen-limited growth of marine phytoplankton. I. Changes in population characteristics with steady-state growth rate. Deep Sea Res 19:601–618. https://doi.org/10.1016/0011-7471(72)90089-7.
5. Falkowski PG. 1997. Evolution of the nitrogen cycle and its influence on

the biological sequestration of $CO_2$ in the ocean. Nature 387:272–275. https://doi.org/10.1038/387272a0.
6. Gruber N. 2004. The dynamics of the marine nitrogen cycle and its influence on atmospheric CO2 variations. *In* Follows M, Oguz T (ed), The ocean carbon cycle and climate. Kluwer Academic, Dordrecht, Netherlands.
7. Gruber N, Galloway JN. 2008. An Earth-system perspective of the global nitrogen cycle. Nature 451:293–296. https://doi.org/10.1038/nature06592.
8. Thompson AW, Zehr JP. 2013. Cellular interactions: lessons from the nitrogen-fixing cyanobacteria. J Phycol 49:1024–1035. https://doi.org/10.1111/jpy.12117.
9. Montoya JP, Holl CM, Zehr JP, Hansen A, Villareal TA, Capone DG. 2004. High rates of $N_2$ fixation by unicellular diazotrophs in the oligotrophic Pacific Ocean. Nature 430:1027–1031. https://doi.org/10.1038/nature02824.
10. Falcón LI, Carpenter EJ, Cipriano F, Bergman B, Capone DG. 2004. $N_2$ fixation by unicellular bacterioplankton from the Atlantic and Pacific oceans: phylogeny and in situ rates. Appl Environ Microbiol 70:765–770. https://doi.org/10.1128/aem.70.2.765-770.2004.
11. Dyhrman ST, Haley ST. 2006. Phosphorus scavenging in the unicellular marine diazotroph *Crocosphaera watsonii*. Appl Environ Microbiol 72:1452–1458. https://doi.org/10.1128/AEM.72.2.1452-1458.2006.
12. Moisander PH, Beinart RA, Hewson I, White AE, Johnson KS, Carlson CA, Montoya JP, Zehr JP. 2010. Unicellular cyanobacterial distributions broaden the oceanic $N_2$ fixation domain. Science 327:1512–1514. https://doi.org/10.1126/science.1185468.
13. Church MJ, Mahaffey C, Letelier RM, Lukas R, Zehr JP, Karl DM. 2009. Physical forcing of nitrogen fixation and diazotroph community structure in the North Pacific subtropical gyre. Global Biogeochem Cycles 23:GB2020. https://doi.org/10.1029/2008GB003418.
14. Webb EA, Ehrenreich IM, Brown SL, Valois FW, Waterbury JB. 2009. Phenotypic and genotypic characterization of multiple strains of the diazotrophic cyanobacterium, *Crocosphaera watsonii*, isolated from the open ocean. Environ Microbiol 11:338–348. https://doi.org/10.1111/j.1462-2920.2008.01771.x.
15. Fu FX, Yu E, Garcia NS, Gale J, Luo Y, Webb EA, Hutchins DA. 2014. Differing responses of marine $N_2$ fixers to warming and consequences for future diazotroph community structure. Aquat Microb Ecol 72:33–46. https://doi.org/10.3354/ame01683.
16. Gallon JR. 1981. The oxygen sensitivity of nitrogenase: a problem for biochemists and micro-organisms. Trends Biochem Sci 6:19–23. https://doi.org/10.1016/0968-0004(81)90008-6.
17. Wang ZC, Burns A, Watt GD. 1985. Complex formation and $O_2$ sensitivity of *Azotobacter vinelandii* nitrogenase and its component proteins. Biochemistry 24:214–221. https://doi.org/10.1021/bi00322a031.
18. Inomura K, Bragg J, Follows MJ. 2017. A quantitative analysis of the direct and indirect costs of nitrogen fixation: a model based on *Azotobacter vinelandii*. ISME J 11:166–175. https://doi.org/10.1038/ismej.2016.97.
19. Mohr W, Intermaggio MP, LaRoche J. 2010. Diel rhythm of nitrogen and carbon metabolism in the unicellular, diazotrophic cyanobacterium *Crocosphaera watsonii* WH8501. Environ Microbiol 12:412–421. https://doi.org/10.1111/j.1462-2920.2009.02078.x.
20. Shi T, Ilikchyan I, Rabouille S, Zehr JP. 2010. Genome-wide analysis of diel gene expression in the unicellular $N_2$-fixing cyanobacterium *Crocosphaera watsonii* WH 8501. ISME J 4:621–632. https://doi.org/10.1038/ismej.2009.148.
21. Saito MA, Bertrand EM, Dutkiewicz S, Bulygin VV, Moran DM, Monteiro FM, Follows MJ, Valois FW, Waterbury JB. 2011. Iron conservation by reduction of metalloenzyme inventories in the marine diazotroph *Crocosphaera watsonii*. Proc Natl Acad Sci 108:2184–2189. https://doi.org/10.1073/pnas.1006943108.
22. Wilson ST, Aylward FO, Ribalet F, Barone B, Casey JR, Connell PE, Eppley JM, Ferrón S, Fitzsimmons JN, Hayes CT, Romano AE, Turk-Kubo KA, Vislova A, Armbrust EV, Caron DA, Church MJ, Zehr JP, Karl DM, Delong EF. 2017. Coordinated regulation of growth, activity and transcription in natural populations of the unicellular nitrogen-fixing cyanobacterium *Crocosphaera*. Nat Microbiol 2. https://doi.org/10.1038/nmicrobiol.2017.118.
23. Garcia HE, Locarnini RA, Boyer TP, Antonov JI, Baranova OK, Zweng MM, Reagan JR, Johnson DR. 2013. Dissolved oxygen, apparent oxygen utilization, and oxygen saturation. *In* Levitus S, Mishonov A (ed), World Ocean Atlas 2013, vol 3. NOAA, Silver Spring, MD.
24. Robertson JE, Watson AJ, Langdon C, Ling RD, Wood JW. 1993. Diurnal variation in surface $pCO_2$ and $O_2$ at 60°N, 20°W in the North Atlantic. Deep Res Part II 40:409–422. https://doi.org/10.1016/0967-0645(93)90024-H.
25. Großkopf T, LaRoche J. 2012. Direct and indirect costs of dinitrogen fixation in *Crocosphaera watsonii* WH8501 and possible implications for the nitrogen cycle. Front Microbiol 3:236. https://doi.org/10.3389/fmicb.2012.00236.
26. Grimaud GM, Rabouille S, Dron A, Sciandra A, Bernard O. 2014. Modelling the dynamics of carbon—nitrogen metabolism in the unicellular diazotrophic cyanobacterium *Crocosphaera watsonii* WH8501, under variable light regimes. Ecol Modell 291:121–133. https://doi.org/10.1016/j.ecolmodel.2014.07.016.
27. Dixon R, Kahn D. 2004. Genetic regulation of biological nitrogen fixation. Nat Rev Microbiol 2:621–631. https://doi.org/10.1038/nrmicro954.
28. Capone DG. 1988. Benthic nitrogen fixation, p 85–123. *In* Blackburn TH, Sorensen J (ed), Nitrogen cycling in coastal marine environments. John Wiley and Sons, New York, NY.
29. Knapp AN. 2012. The sensitivity of marine $N_2$ fixation to dissolved inorganic nitrogen. Front Microbiol 3:374. https://doi.org/10.3389/fmicb.2012.00374.
30. Li WKW. 1980. Temperature adaptation in phytoplankton: cellular and photosynthetic characteristics, p 259–279. *In* Falkowski PG (ed), Primary productivity in the sea. Plenum Press, New York, NY.
31. Geider RJ, Macintyre HL, Kana TM. 1997. Dynamic model of phytoplankton growth and acclimation: responses of the balanced growth rate and the chlorophyll a: carbon ratio to light, nutrient-limitation and temperature. Mar Ecol Prog Ser 148:187–200. https://doi.org/10.3354/meps148187.
32. Cullen JJ. 1990. On models of growth and photosynthesis in phytoplankton. Deep Res 37:667–683. https://doi.org/10.1016/0198-0149(90)90097-F.
33. Geider RJ, Macintyre HL, Kana TM. 1998. A dynamic regulatory model of phytoplanktonic acclimation to light, nutrients, and temperature. Limnol Oceanogr 43:679–694. https://doi.org/10.4319/lo.1998.43.4.0679.
34. Dron A, Rabouille S, Claquin P, Roy B, Talec A, Sciandra A. 2012. Light-dark (12:12) cycle of carbon and nitrogen metabolism in *Crocosphaera watsonii* WH8501: relation to the cell cycle. Environ Microbiol 14:967–981. https://doi.org/10.1111/j.1462-2920.2011.02675.x.
35. Pennebaker K, Mackey KRM, Smith RM, Williams SB, Zehr JP. 2010. Diel cycling of DNA staining and nifH gene regulation in the unicellular cyanobacterium *Crocosphaera watsonii* strain WH 8501 (Cyanophyta). Environ Microbiol 12:1001–1010. https://doi.org/10.1111/j.1462-2920.2010.02144.x.
36. Zehr JP. 2011. Nitrogen fixation by marine cyanobacteria. Trends Microbiol 19:162–173. https://doi.org/10.1016/j.tim.2010.12.004.
37. Sohm JA, Edwards BR, Wilson BG, Webb EA. 2011. Constitutive extracellular polysaccharide (EPS) production by specific isolates of *Crocosphaera watsonii*. Front Microbiol 2:229. https://doi.org/10.3389/fmicb.2011.00229.
38. Inomura K, Bragg J, Riemann L, Follows MJ. 2018. A quantitative model of nitrogen fixation in the presence of ammonium. PLoS One 13:e0208282. https://doi.org/10.1371/journal.pone.0208282.
39. Inomura K, Wilson ST, Deutsch C. 2019. Mechanistic model for the coexistence of nitrogen fixation and photosynthesis in marine Trichodesmium. mSystems 4:e00210-19. https://doi.org/10.1128/mSystems.00210-19.
40. MacDougall JDB, McCabe M. 1967. Diffusion coefficient of oxygen through tissues. Nature 215:1173–1174. https://doi.org/10.1038/2151173a0.
41. Dron A, Rabouille S, Claquin P, Chang P, Raimbault V, Talec A, Sciandra A. 2012. Light:dark (12:12 h) quantification of carbohydrate fluxes in *Crocosphaera watsonii*. Aquat Microb Ecol 68:43–55. https://doi.org/10.3354/ame01600.
42. Vermaas WF. 2001. Photosynthesis and respiration in cyanobacteria, p 245–251. *In* Encyclopedia of life sciences. Macmillan, London, United Kingdom. https://doi.org/10.1038/npg.els.0001670.
43. Sabra W, Zeng AP, Lünsdorf H, Deckwer WD. 2000. Effect of oxygen on formation and structure of *Azotobacter vinelandii* alginate and its role in protecting nitrogenase. Appl Environ Microbiol 66:4037–4044. https://doi.org/10.1128/aem.66.9.4037-4044.2000.
44. Wang D, Xu A, Elmerich C, Ma LZ. 2017. Biofilm formation enables free-living nitrogen-fixing rhizobacteria to fix nitrogen under aerobic conditions. ISME J 11:1602–1613. https://doi.org/10.1038/ismej.2017.30.
45. Cornejo-Castillo FM, Zehr JP. 2019. Hopanoid lipids may facilitate aerobic nitrogen fixation in the ocean. Proc Natl Acad Sci U S A 116:18269–18271. https://doi.org/10.1073/pnas.1908165116.
46. Chen Y-B, Zehr JP, Mellon M. 1996. Growth and nitrogen fixation of the diazotrophic filamentous nonheterocystous cyanobacterium *Trichodesmium* sp. IMS 101 in defined media: evidence for a circadian rhythm. J Phycol 32:916–923. https://doi.org/10.1111/j.0022-3646.1996.00916.x.
47. Nedbal L, Trtílek M, Červený J, Komárek O, Pakrasi HB. 2008. A photobioreactor system for precision cultivation of photoautotrophic micro-

organisms and for high-content analysis of suspension dynamics. Biotechnol Bioeng 100:902–910. https://doi.org/10.1002/bit.21833.
48. Sato T. 1968. A modified method for lead staining of thin sections. J Electron Microsc (Tokyo) 17:158–159.
49. Abràmoff MD, Magalhães PJ, Ram SJ. 2004. Image processing with ImageJ. Biophotonics Int 11:36–42.
50. Capone DG, Montoya JP. 2001. Nitrogen fixation and denitrification. Methods Microbiol 30:501–515. https://doi.org/10.1016/S0580-9517(01)30060-0.
51. Breitbarth E, Mills MM, Friedrichs G, Laroche J. 2004. The Bunsen gas solubility coefficient of ethylene as a function of temperature and salinity and its importance for nitrogen. Limnol Oceanogr Methods 2:282–288. https://doi.org/10.4319/lom.2004.2.282.
52. Masuda T, Bernát G, Bečková M, Kotabová E, Lawrenz E, Lukeš M, Komenda J, Komenda J, Prášil O. 2018. Diel regulation of photosynthetic activity in the oceanic unicellular diazotrophic cyanobacterium *Crocosphaera watsonii* WH8501. Environ Microbiol 20:546–560. https://doi.org/10.1111/1462-2920.13963.
53. Kolber ZS, Prášil O, Falkowski PG. 1998. Measurements of variable chlorophyll fluorescence using fast repetition rate techniques: defining methodology and experimental protocols. Biochim Biophys Acta 1367:88–106. https://doi.org/10.1016/s0005-2728(98)00135-2.
54. Suggett DJ, Prášil O, Borowitzka MA. 2010. Chlorophyll a fluorescence in aquatic sciences: methods and applications. Springer, Dordrecht, Netherlands.
55. Oxborough K, Moore CM, Suggett DJ, Lawson T, Chan HG, Geider RJ. 2012. Direct estimation of functional PSII reaction center concentration and PSII electron flux on a volume basis: a new approach to the analysis of fast repetition rate fluorometry (FRRf) data. Limnol Oceanogr Methods 10:142–154. https://doi.org/10.4319/lom.2012.10.142.
56. Silsbe GM, Oxborough K, Suggett DJ, Forster RM, Ihnken S, Komárek O, Lawrenz E, Prášil O, Röttgers R, Šicner M, Simis SGH, Van Dijk MA, Kromkamp JC. 2015. Toward autonomous measurements of photosynthetic electron transport rates: an evaluation of active fluorescence-based measurements of photochemistry. Limnol Oceanogr Methods 13:138–155.
57. Eilers PHC, Peeters J. 1988. A model for the relationship between light intensity and the rate of photosynthesis in phytoplankton. Ecol Modell 42:199–215. https://doi.org/10.1016/0304-3800(88)90057-9.
58. Silsbe GM, Kromkamp JC. 2012. Modeling the irradiance dependency of the quantum efficiency of photosynthesis. Limnol Oceanogr Methods 10:645–652. https://doi.org/10.4319/lom.2012.10.645.
59. Bühler T, Sann R, Monter U, Dingier C, Kuhla J, Oelze J. 1987. Control of dinitrogen fixation in ammonium-assimilating cultures of *Azotobacter vinelandii*. Arch Microbiol 148:247–251. https://doi.org/10.1007/BF00414820.
60. Benson BB, Krause D. 1984. The concentration and isotopic fractionation of oxygen dissolved in freshwater and seawater in equilibrium with the atmosphere. Limnol Oceanogr 29:620–632. https://doi.org/10.4319/lo.1984.29.3.0620.
61. Fernandez AC, Phillies G. 1983. Temperature dependence of the diffusion coefficient of polystyrene latex spheres. Biopolymers 22:593–595. https://doi.org/10.1002/bip.360220203.
62. Kestin J, Sokolov M, Wakeham WA. 1978. Viscosity of liquid water in the range −8°C to 150°C. J Phys Chem Ref Data 7:941–948. https://doi.org/10.1063/1.555581.